Improving Stereochemical Limitations in Protein-Ligand Complex Structure Prediction

Ryuichiro Ishitani*[a,b], Yoshitaka Moriwaki[a,c]

a. Department of Computational Drug Discovery and Design, Medical Research Laboratory, Institute of Integrated Research, Institute of Science Tokyo, 1-5-45 Yushima, Bunkyo-ku, Tokyo 113-8510, Japan.

b. Department of Biological Sciences, Graduate School of Science, The University of Tokyo, 7-3-1 Hongo, Bunkyo-ku, Tokyo 113-0033, Japan.

c. Graduate School of Agricultural and Life Sciences, The University of Tokyo, 1-1-1 Yayoi, Bunkyo-ku, Tokyo 113-8657, Japan.

* Corresponding author.

Abstract

AlphaFold3 has revolutionized biology by enabling the prediction of protein complexes with various biomolecules, including small molecular ligands. However, the ligand structures predicted by the model often contain stereochemical errors. In this study, our comprehensive evaluation of AlphaFold3 and its clone model, Boltz-1, demonstrated significant limitations in ligand stereochemistry of their predicted structures, including chirality, bond, and angle geometries. To address the issue, we developed the restraint-guided inference method that applies stereochemical restraints during the reverse diffusion process. This approach perfectly reproduces the chirality specified in the input chemical structure and improves bond and angle geometries of ligands, while maintaining comparable performance in binding pose prediction. Our method provides a practical solution to the stereochemical errors in predicting protein-ligand complexes, thereby enhancing applications of structure prediction in structural biology and drug discovery. The materials supporting this article, including the source code and Colab notebook are available at github (https://github.com/cddlab/boltz_ext and https://github.com/cddlab/colabfold_boltz_restr).

Introduction

The field of protein structure prediction has experienced revolutionary advancements in recent years. Notably, AlphaFold2, introduced by DeepMind in 2021, demonstrated unprecedented accuracy in predicting protein structures[1]. Following this, AlphaFold3 has expanded its capabilities beyond traditional protein structure prediction to include the structural determination of heterogeneous complexes involving RNA, DNA, glycans, and small molecular ligands[2]. These remarkable contributions have received significant recognition within the scientific community and have been awarded the 2024 Nobel Prize in Chemistry. Several derivative models, such as Boltz-1[3], Protenix[4], Chai-1[5], and HelixFold3[6], have also been developed.

AlphaFold3 employs a diffusion model approach, allowing it to predict structures for various biological molecules. In particular, concerning the prediction of protein-ligand complexes, the AlphaFold3 paper claims that it can achieve greater accuracy than conventional molecular docking methods[2]. However, several issues remain to be addressed before it can be used as a substitute for conventional molecular docking methods. For example, it has been reported that the predicted ligand structure sometimes contains stereochemistry violations[2], including errors with chirality, despite the correct reference structure given to the input features. These challenges could pose significant limitations for applications in biological research, including drug design and biosynthesis.

In this study, we first evaluate the structure prediction of protein-ligand complexes by AlphaFold3[2] and its clone Boltz-1[3], mainly focusing on the stereochemistry of ligands. Our analysis reveals that both models often failed to reproduce the local conformations and chirality of ligands specified by the input. Then, we propose a novel method to

address the issues of chirality and local conformation prediction without retraining the model. By applying this approach, we achieve a 100% success rate in chirality reproduction. This research elucidates the limitations of structure prediction models and provides a practical solution to overcome these problems.

Methods

Benchmark dataset

We evaluated the accuracy of protein-ligand complex structure prediction using AlphaFold3[2] and its clone model, Boltz-1[3]. Both prediction models utilize a "reference conformer" as one of their input features. When the chemical structure of the ligand is provided in SMILES notation or Chemical Component Dictionary (CCD) code, its three-dimensional structure (conformer) is generated using ETKDGv3 algorithm[7] implemented in RDKit and then used as the reference conformer. This study systematically assessed how accurately the stereochemistry—specifically the chiralities, bond lengths, and bond angles—of the reference conformer is reproduced in the predicted structures.

To evaluate the stereochemistry of the ligands in the predicted structures, we utilized entries extracted from the PDBBind2020 dataset[8]. The criteria for selecting entries to construct the evaluation dataset were as follows:

1. Entries where proteins do not form multimers.
2. Entries containing one ligand that is not a polymer and thus can be represented by a single CCD code.
3. Entries with a ligand containing at least one chiral center at an sp^3-hybridized carbon atom.
4. Entries where the non-hydrogen atoms of the ligand consist solely of the elements C, N, O, F, P, S, Cl, Br, and I.
5. Entries containing a ligand whose reference conformer can be generated by RDKit.

By applying these criteria, we extracted 4,500 entries. This dataset may contain structures that are also part of the training data for AlphaFold3 and Boltz-1. We purposely

retained these entries in our evaluation dataset because our main objective is to assess whether the models can accurately reproduce the stereochemistry of the "reference conformers" in the input features, including those in the training dataset. The prediction of the ligand structures in the training dataset should be easier than that of novel compounds. Thus, we hypothesized that if the models had memorized the training data, they could reproduce the structures accurately.

Evaluation metrics

We created RDKit Mol objects from the SMILES notation found in the CCD and assigned conformers, including chirality, based on the three-dimensional structures of the compounds in the PDBbind2020 dataset. Using these RDKit Mol objects, we enumerated chiral centers and examined the R/S chirality of each atom according to the Cahn–Ingold–Prelog (CIP) priority rules implemented in RDKit[9]. We then assessed the chirality of the corresponding atoms in the predicted structures and evaluated their consistency. If even one atom exhibited a different chirality, we recorded it as inconsistent and evaluated the fraction of consistent molecules against the total entries. To simplify the problem, we focused solely on the chirality of sp^3 carbon atoms, which are commonly found in biomolecules.

We further evaluated the deviation of the predicted structures from the reference conformer in terms of their bond lengths and angles. Specifically, we calculated the root mean square of the deviations (RMSDs) from the ideal bond lengths ($\hat{r}_i$) and angles ($\hat{\theta}_i$) of the reference conformers generated by ETKDGv3 algorithm of RDKit[7].

$$\text{BondRMSD} = \sqrt{\frac{1}{N_b}\sum_{i}^{N_b}(r_i - \hat{r}_i)^2}$$

$$\text{AngleRMSD} = \sqrt{\frac{1}{N_a}\sum_{i}^{N_a}\left(\theta_i - \hat{\theta}_i\right)^2}$$

To assess the accuracy of ligand binding site predictions, we performed a least-squares superposition of protein residues within 10 Å of the ligand binding site and calculated the RMSD of the corresponding ligand atoms, as described in the AlphaFold3 paper[2].

Improvement of geometry through restraints

To overcome the stereochemistry violation problems described in the AlphaFold3 paper[2], we developed a novel approach in this study. Instead of modifying or retraining the neural network model, we attempted to alter the diffusion model's inference process to utilize chirality information, bond lengths, and bond angles as restraints. Our method was inspired by the symmetry-guided generation approach used in RFDiffusion[10]. In RFDiffusion, symmetric multimer protein structures are generated by applying hard constraints to protein Cα atoms at each step to enforce the desired symmetry. Similarly, we adopted an approach that applies restraints related to compound stereochemistry to the structures at each step of the reverse diffusion process. This method aims to accurately predict compound stereochemistry without requiring model retraining.

The diffusion model used in AlphaFold3 is the EDM[11]. In each inference step i of EDM, the next step sample $\boldsymbol{x}_{i+1}$ is calculated using the difference $\boldsymbol{d}_i$ computed from the

output of the denoiser function D_θ and the current step sample $\hat{\boldsymbol{x}}_i$:

$$\hat{t}_i = t_i + \gamma_i t_i$$

$$\hat{\boldsymbol{x}}_i = \boldsymbol{x}_i + \lambda\sqrt{\hat{t}_i^2 - t_i^2} \cdot \mathcal{N}(\mathbf{0}, \mathbf{I}_3)$$

$$\boldsymbol{y}_i = D(\hat{\boldsymbol{x}}_i; \hat{t}_i)$$

$$\boldsymbol{x}_{i+1} = \hat{\boldsymbol{x}}_i + \eta(t_{i+1} - \hat{t}_i)\,(\hat{\boldsymbol{x}}_i - \boldsymbol{y}_i)/\hat{t}_i$$

where, γ_i, λ, and η are hyperparameters to control the stochasticity levels.

To achieve denoising based on the training dataset, D is implemented through a neural network D_θ with a parameter set θ. This $\boldsymbol{x}_{i+1}$ is influenced by the noise scale and exhibits a distribution significantly different from the actual coordinate scale. This discrepancy makes applying restraints directly to $\boldsymbol{x}_{i+1}$ impractical. In contrast, it was shown that the optimal denoising function D, which analytically minimizes the training objective, converges toward the mean of the dataset as the noise level increases. Conversely, as the noise level decreases, it approaches the ground truth of the dataset (see Equation B.3, eq. 57 in ref[11]). Consequently, the output of D_θ is expected to remain consistent with the scale of the samples (i.e., experimental structures) present in the training dataset. Therefore, we implemented a method where stereochemical restraints based on the input reference conformer are applied to $\boldsymbol{y}_i$ to obtain $\tilde{\boldsymbol{y}}_i$, and then the difference between $\hat{\boldsymbol{x}}_i$ and $\tilde{\boldsymbol{y}}_i$ is used for calculating $\boldsymbol{x}_{i+1}$ for the subsequent step. These constrained reverse diffusion steps are applied when the condition $t_{i+1} < \sigma_{\text{start}}$ is satisfied, where σ_{start} is an input parameter.

Implementation of the restraints

In this study, we implemented stereochemical restraints targeting chirality of sp^3

carbon atoms, bond lengths, and bond angles. These parameters typically do not deviate significantly from their ideal values calculated from the chemical structures when compounds are bound to the target protein molecules. In contrast, parameters such as dihedral angles can undergo substantial changes during protein-ligand binding processes and are therefore excluded from our restraint targets.

To maintain the correct chirality, we constrained the chiral volume to its ideal value. The chiral volume ($V_i(j,k,l)$) for the chiral center atom (i) was calculated by the following formula:

$$V_i(j,k,l) = \left(\vec{\boldsymbol{x}}_i - \vec{\boldsymbol{x}}_j\right) \cdot \left((\vec{\boldsymbol{x}}_i - \vec{\boldsymbol{x}}_k) \times (\vec{\boldsymbol{x}}_i - \vec{\boldsymbol{x}}_l)\right)$$

where the atoms j, k, l are adjucent atoms directly connected to atom i by covalent bonds. Then, the chirality restraints are achieved by minimizing the following term:

$$L_{\text{chiral}}(\{\vec{\boldsymbol{x}}\}) = \sum_{i \in \text{chiral centers}} \left(V_i - V_i^{\text{ref}}\right)^2$$

where V_i represents the calculated chiral volume of the chiral center i, and V_i^{ref} is the reference value obtained from the input reference conformer. It is important to maintain the same order of j, k, and l in the above formula for both the current structure (V_i) and the reference conformer (V_i^{ref}) to preserve the same chirality.

For constraining bond lengths and bond angles within the compound, we minimized the following terms:

$$L_{\text{bond}}(\{\vec{\boldsymbol{x}}\}) = \sum_{i,j \in \text{bonds}} \left(d_{ij} - d_{ij}^{\text{ref}}\right)^2$$

$$L_{\text{angle}}(\{\vec{\boldsymbol{x}}\}) = \sum_{i,j,k \in \text{angles}} \left(\theta_{ijk} - \theta_{ijk}^{\text{ref}}\right)^2$$

where d_{ij} denotes the bond length between atoms i and j, and θ_{ijk} represents the bond angle formed by atoms i, j, and k. The reference values d_{ij}^{ref} and $\theta_{ijk}^{\text{ref}}$ were derived from the input reference conformer.

The final restraint implementation was achieved by minimizing a weighted sum of the individual terms:

$$L_{\text{total}}(\{\vec{\boldsymbol{x}}\}) = w_{\text{chiral}} \cdot L_{\text{chiral}} + w_{\text{geom}} \cdot (L_{\text{bond}} + L_{\text{chiral}})$$

$$\tilde{\boldsymbol{y}}_i = \underset{\vec{\boldsymbol{x}} \in \mathcal{N}(\boldsymbol{y}_i)}{\operatorname{argmin}} L_{\text{total}}(\{\vec{\boldsymbol{x}}\})$$

where w_{chiral} and w_{geom} are weighting coefficients for each corresponding term. We implemented this method in Boltz-1[3], a PyTorch-based clone of AlphaFold3. The minimization was performed using the conjugate gradient method implemented in the SciPy optimization library[12].

Multiple Sequence Alignment and Structure Prediction

Multiple sequence alignments used for structure prediction were pre-computed for each amino acid sequence using MMSeqs2 v15[13] and localcolabfold[14]. The same alignments were used across all three methods: AlphaFold3, Boltz-1, and Boltz-1 with restraints. For AlphaFold3 predictions, we used the default input parameters. In the case of Boltz-1, to maintain consistency with AlphaFold3 conditions, we preformed predictions with settings of recycle=10 and nsamples=5. All calculations were performed using NVIDIA GeForce RTX 4090 GPUs.

Results

Benchmark of protein-ligand complex structure prediction

In this study, we evaluated the protein-ligand complex prediction capabilities of

AlphaFold3 (AF3)[2] and Boltz-1[3] using 4,500 entries derived from the PDBbind2020 dataset[8]. Both models demonstrated excellent performance in predicting the protein structures, with RMSDs of around 0.6 Å (Table 1). As far as evaluating from the Ligand RMSD, the prediction performance of the ligand structure also appeared promising, with values below 2.0 Å for AF3. However, as mentioned in the Methods section, our evaluation dataset was not created with consideration of overlapping with the training dataset. Therefore, these results should not be interpreted as reflecting model performance against entirely novel compounds or binding pockets.

Regarding the stereochemistry of the predicted ligand structures, we found an issue in reproducing the chirality of input molecules (Table 1). One possible reason for this stereochemistry issue may stem from the ligand atom names used to create the input features. The atom names differ between the inputs generated using CCD code and those in SMILES notation. As a result, the input features can vary even for identical ligands, which might impact performance. To explore this hypothesis, we also compared the prediction results using CCD codes and found that chirality reproduction improved slightly (from 78.6% to 79.4%). This aligns with the fact that the atom names from CCD are used during model training. However, a significant number of ligands still exhibited stereochemical errors.

A comparison of the results from AF3 and Boltz-1 revealed that AF3 showed superior performance in chirality reproduction, bond/angle RMSD, and ligand RMSD (Table 1). Overall, while AF3 generates higher-quality predicted structures than Boltz-1, both models still face challenges regarding ligand stereochemistry.

Structure prediction using the restraint-guided inference

We also evaluated the prediction accuracy of Boltz-1 with the restraint-guided inference proposed in this study. This inference method involves multiple hyperparameters (σ_{start}, w_{chiral}, and w_{geom}), so we assessed the model's performance under several conditions (Table 1). Specifically, we conducted experiments where restraints were applied at the final step ($\sigma_{\text{start}} = 0.05$; Boltz R1) and during the last 55 steps ($\sigma_{\text{start}} = 1$; Boltz R) of the 200-step reverse diffusion process. Furthermore, we compared experiments that applied restraints only to the chiral volume ($w_{\text{chiral}} = 1$ and $w_{\text{geom}} = 0$; Boltz RC) against those that applied restraints to all parameters: chiral volume, bond length, and bond angle ($w_{\text{chiral}} = w_{\text{geom}} = 1$; Boltz R).

The results showed that the chirality of the input molecule was reproduced 100% across all conditions with restraints except for Boltz R1, in which a small fraction of the chirality inversion was observed (Table 1). These findings emphasize the importance of applying restraints iteratively within the reverse diffusion process. Additionally, results from Boltz-RC, which applied restraints solely on the chiral volumes, demonstrated that accurate chirality could be achieved by constraining only the chiral volume (Table 1).

We then evaluated the bond and angle RMSD values for each prediction result. Under the Boltz R1 conditions, these values became worse compared to those from the model without restraints (Table 1, Fig 1B, C). This finding is consistent with the reproducibility of chirality, further showing the importance of applying multiple restraint steps. In contrast, under Boltz RC conditions where restraints were applied only to the chiral volumes, the bond and angle RMSD values were comparable to those from the model without restraints (Table 1, Fig 1B, C). Thus, applying restraints on the chiral

volumes does not adversely affect the bond length and angle geometries. One particularly notable finding was that under Boltz-R conditions, where restraints were applied to all parameters (i.e., chiral volume, bond length, and angle), the bond and angle RMSD values showed significant improvement. They exceeded the values achieved by AF3 (Table 1, Fig 1B, C). This result again underscores that our method can accurately reproduce the stereochemical properties of the input reference conformers.

Case study for chirality reproducibility of ligands

Next, we explored specific instances where the chirality of ligands differed from that in the input reference conformer. In the angiotensin-converting enzyme and inhibitor complex (PDB ID: 4BXK)[15], the chirality of one carbon atom was predicted to be different from that in the reference conformer (Fig. 2). We also analyzed the case where the ligand was specified by the CCD code. The resulting output structure also exhibited a different chirality from that in the input, exemplifying that the reproducibility of chirality was not improved using the atom name assignments derived from CCD (Fig. 2C). In contrast, the Boltz R result with restraint-guided inference produced a structure with the correct chirality (Fig. 2E). A comparison of the predicted structures showed that the Boltz-R result superposes better with the experimental structure than those by Boltz-1 or AF3 (Fig. 2A, E). However, when measured by Ligand RMSD, AF3 and Boltz R exhibited similar values of 0.38 Å and 0.39 Å, respectively. The changes in the atomic positions due to the chirality change are not substantial, which are averaged out when evaluating RMSD. This result may explain why there were no significant changes in the distribution of ligand RMSD despite improvements in chirality by the restraint-guided inference (Fig

1A).

We also investigated the specific example of Cα carbon atom chirality in amino acid ligands. In the case of the glutamate transporter and D-aspartate complex (PDB ID: 6R7R)[16], both AF3 and Boltz-1 predicted conformations corresponding to the L-form amino acid (Fig. 3). Using CCD code to conform to the atom name nomenclature of amino acids (*i.e.*, CA, CB, etc.) did not improve the results (Fig. 3C). In contrast, with the restraint-guided inference, Boltz-R predicted the structure with the correct chirality (Fig 3A, E). Similar results were also observed in other complex structures with D-form amino acids. These findings demonstrate that when the ligands resemble the monomers of biopolymers, such as L-amino acids in proteins or riboses in nucleic acids, AF3 and Boltz-1 tend to alter their chirality to match that of these biopolymers. While the input atom embeddings of AF3 include information on the atom names, elements, and formal charges, they lack specific information about the chiral centers. Consequently, the model cannot learn the relationship between the atom representations and the arrangement of substituents around the sp^3-carbon atoms.

Case study for bond and angle geometries of ligands

Next, we investigated specific cases where the bond and angle RMSDs of the ligand structures predicted by AF3 and Boltz-1 showed significant deterioration. In these cases, we observed several inconsistencies between the predicted ligand conformers and the reference conformers, including:

1. Structural inconsistencies in aromatic and non-aromatic rings
2. Hybridization state inconsistencies in non-cyclic structures

For the first case, we examined the ectoine-binding protein UehA complexed with ectoine (PDB ID: 3FXB)[17]. In the structures predicted by AF3 and Boltz-1, the ligand's ring structure was incorrectly modeled as planar, while the reference conformer contains a non-aromatic saturated ring (Fig. 4A-D). This error likely occurs because the chemical structure of the ring resembles that of pyrimidine nucleobase, which is commonly found in the training data. This similarity causes the model to predict it as an aromatic structure incorrectly. For the second case, we examined the FimH lectin domain complexed with a small molecule (PDB ID: 4AV4)[18]. In the prediction structure by AF3 and Boltz-1, the sp^1 carbon atoms of the alkyne group in the ligand, which should form a linear structure, is instead predicted as an sp^3 alkyl chain-like structure (Fig. 4E-H). This observation suggests that structures rarely found in natural biomolecules, such as sp^1 carbons, are biased toward frequently occurring structures like sp^3 carbons, resulting in predicted ligand structures with incorrect stereochemistry.

These problems may stem from fundamental limitations in the input feature representation of the AF3 model. Specifically, the atom and bond embeddings in AF3 do not include explicit information about hybridization states, as well as bond orders, such as single or double bonds. As a result, chemically distinct atoms and bonds are treated as similar input features. This leads the model to skew predictions toward structural patterns frequently occurring in the training dataset. The cases discussed here illustrate stereochemical errors likely caused by this input embedding issues. Even in such cases, our restraint-guided inference strategy successfully generated structures with correct stereochemical properties (Fig. 4D, H). These results underscore that the proposed method effectively overcame the limitations of AF3 and Boltz-1 in ligand stereochemistry.

Discussion

In this study, we comprehensively investigated stereochemical accuracy in protein-ligand complex structure predictions by AlphaFold3 and its clone model Boltz-1, using unified assessment criteria against the same benchmark dataset. Our results confirmed that the ligands of the predicted structures contain significant levels of stereochemical errors in their chiralities, bond lengths, and angles. Then, we developed the restraint-guided inference method to address these stereochemical errors. Our evaluation confirmed that this method effectively improves the stereochemical validity of the ligand structures. Importantly, we demonstrated that the restraint-guided inference method does not adversely affect the performance of the binding pose prediction.

We focused on the method to address the stereochemical errors without retraining the model in this study. However, as discussed in the Results section, one potential cause of the ligand stereochemistry violations may arise from using feature representations, such as atom names, which can vary depending on the input notations. Therefore, a fundamental solution would require a model design that directly incorporates invariant features of compound structures, including hybridization states, chirality, and bond orders.

In the current models, natural biomolecules such as protein amino acids, nucleic acids, and glycans rarely experience those stereochemical issues. This is likely because these molecules are abundant in their training dataset. Therefore, a similar solution could theoretically be possible for small organic compounds by including sufficient numbers and diversity in the training dataset. However, the chemical space of small molecules is orders of magnitude larger than the limited set of biomolecular building blocks, making it impractical to train the neural network model to correctly preserve stereochemistry

across arbitrary compounds. From this perspective, our approach provides a practical solution for the ligand stereochemistry problems.

Author contributions

R.I. designed the study and analyzed the data. R.I., and Y.M. performed computational experiments and wrote the manuscript. R.I. directed and supervised this study.

Acknowledgements

This research was partially supported by Research Support Project for Life Science and Drug Discovery (Basis for Supporting Innovative Drug Discovery and Life Science Research (BINDS)) from AMED under Grant Number JP23ama121028 for K.T. and JP24ama121012 for R.I. This work partly used computational resources of supercomputer "Flow" provided by Information Technology Center, Nagoya University, through the HPCI System Research Project (Project ID: hp240040).

Data and Software Availability

The materials supporting this article, including the source code and Colab notebook are available at github (https://github.com/cddlab/boltz_ext and https://github.com/cddlab/colabfold_boltz_restr/blob/main/Boltz1.ipynb).

Figures

Figure 1

Distribution of metrics for the ligands in the predicted structures from the dataset used in this study. Panels (A)-(C) illustrate the distributions of (A) Ligand RMSD, (B) Bond RMSD, and (C) Angle RMSD values. The left panels compare the results from Boltz-R, Boltz-1, and AF3, while the right panels compare Boltz-R, Boltz-1, Boltz-RC, and Boltz-R1.

Figure 2

An example showing the chirality issue in the small molecule compounds. (A) The experimental structure of the angiotensin-converting enzyme and its inhibitor complex (PDB ID: 4BXK) is compared with predictions from: (B) AlphaFold3, (C) AlphaFold3 using CCD code (1IU), (D) Boltz-1, and (E) Boltz-1 with restraint-guided inference. Ligands are represented as ball-and-stick models, while proteins are shown as ribbon diagrams. Chiral centers within the ligands are highlighted in red.

Figure 3

An example showing the chirality issue in the D-amino acid ligands. (A) The experimental structure of the glutamate transporter in complex with D-aspartate (PDB ID: 6R7R) is compared to predictions from (B) AlphaFold3, (C) AlphaFold3 with CCD ligand code, (D) Boltz-1, and (E) Boltz-1 using restraint-guided inference. Ligands are

represented as ball-and-stick models, while proteins are depicted as ribbons. Chiral centers within the ligands are highlighted in red.

Figure 4

Examples showing changes in ligand bond and angle geometries from reference conformers. (A-D) Ectoine-binding protein UehA complex with ectoine (PDB: 3FXB). (A) Experimental structure compared with predictions from (B) AlphaFold3, (C) Boltz-1, and (D) Boltz-1 with restraint guidance. (E-H) FimH lectin domain complex with a small molecule (PDB: 4AV4). (E) Experimental structure compared with predictions from (F) AlphaFold3, (G) Boltz-1, and (H) Boltz-1 with restraint guidance. All panels show ligands as ball-and-stick models with oxygen atoms in red and nitrogen atoms in blue. Proteins are displayed as ribbon models.

Tables

Table 1

Evaluation metrics for proteins and ligands in the predicted structures from the dataset used in this study.

	Conditions	Protein RMSD (Å)	Chirality (%)	Bond RMSD (Å)	Angle RMSD (°)	Ligand RMSD (Å)
AF3		0.660	78.6	0.0196	0.244	1.871
Boltz-1		0.629	67.6	0.0303	0.650	2.534
Boltz R1	$\sigma_{\text{start}} = 0.05, w_{\text{chiral}} = w_{\text{geom}} = 1$	0.624	99.9	0.0494	1.306	2.550
Boltz RC	$\sigma_{\text{start}} = 1, w_{\text{chiral}} = 1, w_{\text{geom}} = 0$	0.628	100	0.0234	0.509	2.537
Boltz R	$\sigma_{\text{start}} = 1, w_{\text{chiral}} = w_{\text{geom}} = 1$	0.628	100	0.0005	0.044	2.516

References

(1) Jumper, J.; Evans, R.; Pritzel, A.; Green, T.; Figurnov, M.; Ronneberger, O.; Tunyasuvunakool, K.; Bates, R.; Žídek, A.; Potapenko, A.; Bridgland, A.; Meyer, C.; Kohl, S. A. A.; Ballard, A. J.; Cowie, A.; Romera-Paredes, B.; Nikolov, S.; Jain, R.; Adler, J.; Back, T.; Petersen, S.; Reiman, D.; Clancy, E.; Zielinski, M.; Steinegger, M.; Pacholska, M.; Berghammer, T.; Bodenstein, S.; Silver, D.; Vinyals, O.; Senior, A. W.; Kavukcuoglu, K.; Kohli, P.; Hassabis, D. Highly Accurate Protein Structure Prediction with AlphaFold. *Nature* **2021**, *596* (7873), 583–589.

(2) Abramson, J.; Adler, J.; Dunger, J.; Evans, R.; Green, T.; Pritzel, A.; Ronneberger, O.; Willmore, L.; Ballard, A. J.; Bambrick, J.; Bodenstein, S. W.; Evans, D. A.; Hung, C.-C.; O'Neill, M.; Reiman, D.; Tunyasuvunakool, K.; Wu, Z.; Žemgulytė, A.; Arvaniti, E.; Beattie, C.; Bertolli, O.; Bridgland, A.; Cherepanov, A.; Congreve, M.; Cowen-Rivers, A. I.; Cowie, A.; Figurnov, M.; Fuchs, F. B.; Gladman, H.; Jain, R.; Khan, Y. A.; Low, C. M. R.; Perlin, K.; Potapenko, A.; Savy, P.; Singh, S.; Stecula, A.; Thillaisundaram, A.; Tong, C.; Yakneen, S.; Zhong, E. D.; Zielinski, M.; Žídek, A.; Bapst, V.; Kohli, P.; Jaderberg, M.; Hassabis, D.; Jumper, J. M. Accurate Structure Prediction of Biomolecular Interactions with AlphaFold 3. *Nature* **2024**, *630* (8016), 493–500.

(3) Wohlwend, J.; Corso, G.; Passaro, S.; Reveiz, M.; Leidal, K.; Swiderski, W.; Portnoi, T.; Chinn, I.; Silterra, J.; Jaakkola, T.; Barzilay, R. Boltz-1 Democratizing Biomolecular Interaction Modeling. *bioRxivorg*, 2024, 2024.11.19.624167. https://doi.org/10.1101/2024.11.19.624167.

(4) Chen, X.; Zhang, Y.; Lu, C.; Ma, W.; Guan, J.; Gong, C.; Yang, J.; Zhang, H.; Zhang,

K.; Wu, S.; Zhou, K.; Yang, Y.; Liu, Z.; Wang, L.; Shi, B.; Shi, S.; Xiao, W. Protenix - Advancing Structure Prediction through a Comprehensive AlphaFold3 Reproduction. *bioRxiv*, 2025, 2025.01.08.631967. https://doi.org/10.1101/2025.01.08.631967.

(5) Boitreaud, J.; Dent, J.; McPartlon, M.; Meier, J.; Reis, V.; Rogozhnikov, A.; Wu, K. Chai-1: Decoding the Molecular Interactions of Life. *Synthetic Biology*, 2024. https://www.biorxiv.org/content/10.1101/2024.10.10.615955v1.full.pdf.

(6) Liu, L.; Zhang, S.; Xue, Y.; Ye, X.; Zhu, K.; Li, Y.; Liu, Y.; Gao, J.; Zhao, W.; Yu, H.; Wu, Z.; Zhang, X.; Fang, X. Technical Report of HelixFold3 for Biomolecular Structure Prediction. *arXiv [q-bio.BM]*, 2024. http://arxiv.org/abs/2408.16975 (accessed 2025-03-14).

(7) Wang, S.; Witek, J.; Landrum, G. A.; Riniker, S. Improving Conformer Generation for Small Rings and Macrocycles Based on Distance Geometry and Experimental Torsional-Angle Preferences. *J. Chem. Inf. Model.* **2020**, *60* (4), 2044–2058.

(8) Liu, Z.; Li, Y.; Han, L.; Li, J.; Liu, J.; Zhao, Z.; Nie, W.; Liu, Y.; Wang, R. PDB-Wide Collection of Binding Data: Current Status of the PDBbind Database. *Bioinformatics* **2015**, *31* (3), 405–412.

(9) Hanson, R. M.; Musacchio, S.; Mayfield, J. W.; Vainio, M. J.; Yerin, A.; Redkin, D. Algorithmic Analysis of Cahn-Ingold-Prelog Rules of Stereochemistry: Proposals for Revised Rules and a Guide for Machine Implementation. *J. Chem. Inf. Model.* **2018**, *58* (9), 1755–1765.

(10) Watson, J. L.; Juergens, D.; Bennett, N. R.; Trippe, B. L.; Yim, J.; Eisenach, H. E.; Ahern, W.; Borst, A. J.; Ragotte, R. J.; Milles, L. F.; Wicky, B. I. M.; Hanikel, N.; Pellock, S. J.; Courbet, A.; Sheffler, W.; Wang, J.; Venkatesh, P.; Sappington, I.;

Torres, S. V.; Lauko, A.; De Bortoli, V.; Mathieu, E.; Ovchinnikov, S.; Barzilay, R.; Jaakkola, T. S.; DiMaio, F.; Baek, M.; Baker, D. De Novo Design of Protein Structure and Function with RFdiffusion. *Nature* **2023**, *620* (7976), 1089–1100.

(11) Karras, T.; Aittala, M.; Aila, T.; Laine, S. Elucidating the Design Space of Diffusion-Based Generative Models. *arXiv [cs.CV]*, 2022. http://arxiv.org/abs/2206.00364 (accessed 2025-03-14).

(12) Virtanen, P.; Gommers, R.; Oliphant, T. E.; Haberland, M.; Reddy, T.; Cournapeau, D.; Burovski, E.; Peterson, P.; Weckesser, W.; Bright, J.; van der Walt, S. J.; Brett, M.; Wilson, J.; Millman, K. J.; Mayorov, N.; Nelson, A. R. J.; Jones, E.; Kern, R.; Larson, E.; Carey, C. J.; Polat, İ.; Feng, Y.; Moore, E. W.; VanderPlas, J.; Laxalde, D.; Perktold, J.; Cimrman, R.; Henriksen, I.; Quintero, E. A.; Harris, C. R.; Archibald, A. M.; Ribeiro, A. H.; Pedregosa, F.; van Mulbregt, P.; SciPy 1.0 Contributors. SciPy 1.0: Fundamental Algorithms for Scientific Computing in Python. *Nat. Methods* **2020**, *17* (3), 261–272.

(13) Steinegger, M.; Söding, J. MMseqs2 Enables Sensitive Protein Sequence Searching for the Analysis of Massive Data Sets. *Nat. Biotechnol.* **2017**, *35* (11), 1026–1028.

(14) Mirdita, M.; Schütze, K.; Moriwaki, Y.; Heo, L.; Ovchinnikov, S.; Steinegger, M. ColabFold: Making Protein Folding Accessible to All. *Nat. Methods* **2022**, *19* (6), 679–682.

(15) Douglas, R. G.; Sharma, R. K.; Masuyer, G.; Lubbe, L.; Zamora, I.; Acharya, K. R.; Chibale, K.; Sturrock, E. D. Fragment-Based Design for the Development of N-Domain-Selective Angiotensin-1-Converting Enzyme Inhibitors. *Clin. Sci. (Lond.)* **2014**, *126* (4), 305–313.

(16) Arkhipova, V.; Trinco, G.; Ettema, T. W.; Jensen, S.; Slotboom, D. J.; Guskov, A.

Binding and Transport of D-Aspartate by the Glutamate Transporter Homolog GltTk. *Elife* **2019**, *8*. https://doi.org/10.7554/eLife.45286.

(17) Lecher, J.; Pittelkow, M.; Zobel, S.; Bursy, J.; Bönig, T.; Smits, S. H. J.; Schmitt, L.; Bremer, E. The Crystal Structure of UehA in Complex with Ectoine-A Comparison with Other TRAP-T Binding Proteins. *J. Mol. Biol.* **2009**, *389* (1), 58–73.

(18) Wellens, A.; Lahmann, M.; Touaibia, M.; Vaucher, J.; Oscarson, S.; Roy, R.; Remaut, H.; Bouckaert, J. The Tyrosine Gate as a Potential Entropic Lever in the Receptor-Binding Site of the Bacterial Adhesin FimH. *Biochemistry* **2012**, *51* (24), 4790–4799.

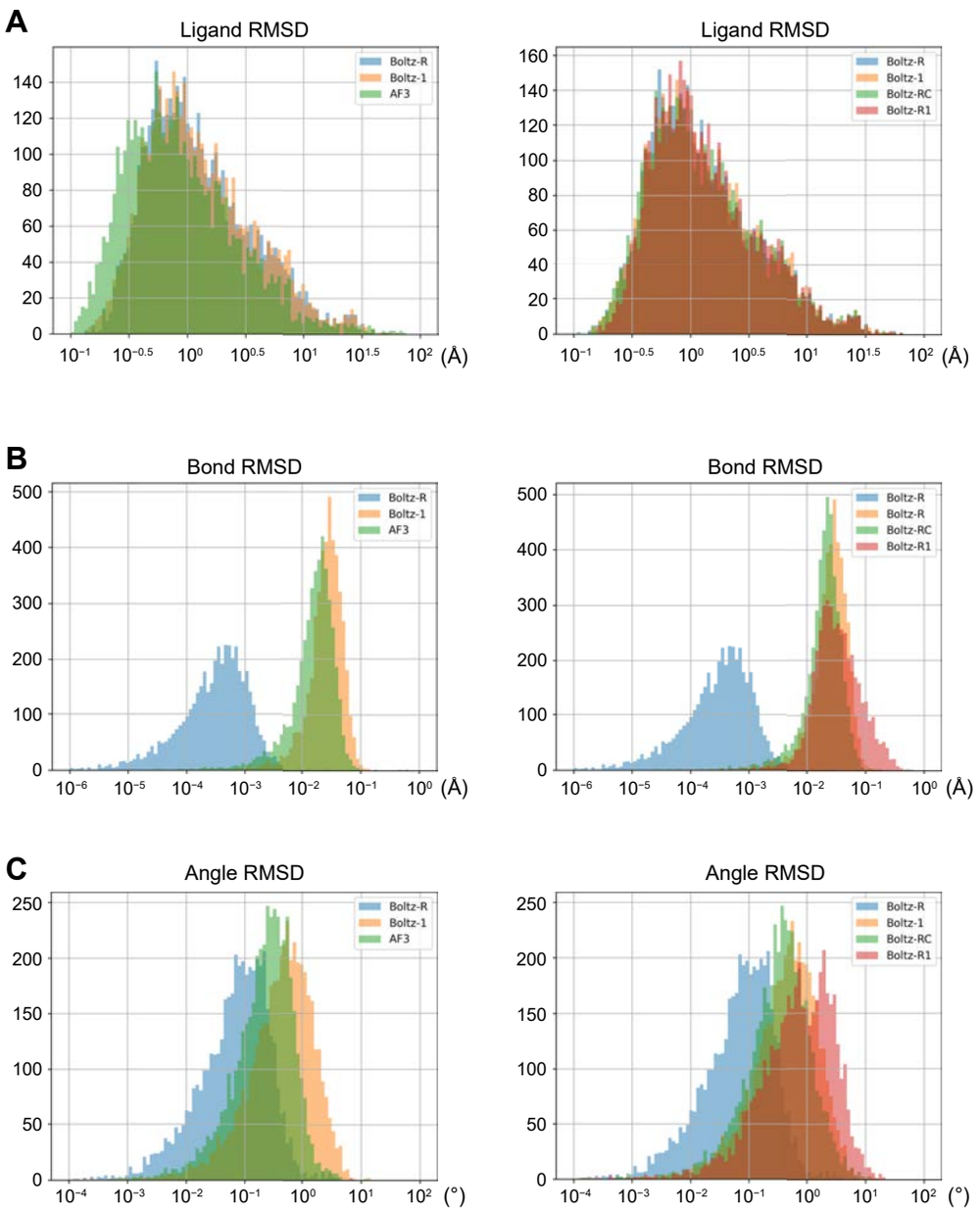
A
Ligand RMSD
Boltz-R
Boltz-1
AF3
Ligand RMSD
Boltz-R
Boltz-1
Boltz-RC
Boltz-R1
(Å)
B
Bond RMSD
Boltz-R
Boltz-1
AF3
Bond RMSD
Boltz-R
Boltz-R
Boltz-RC
Boltz-R1
(Å)
C
Angle RMSD
Boltz-R
Boltz-1
AF3
Angle RMSD
Boltz-R
Boltz-1
Boltz-RC
Boltz-R1
(°)

Fig 1

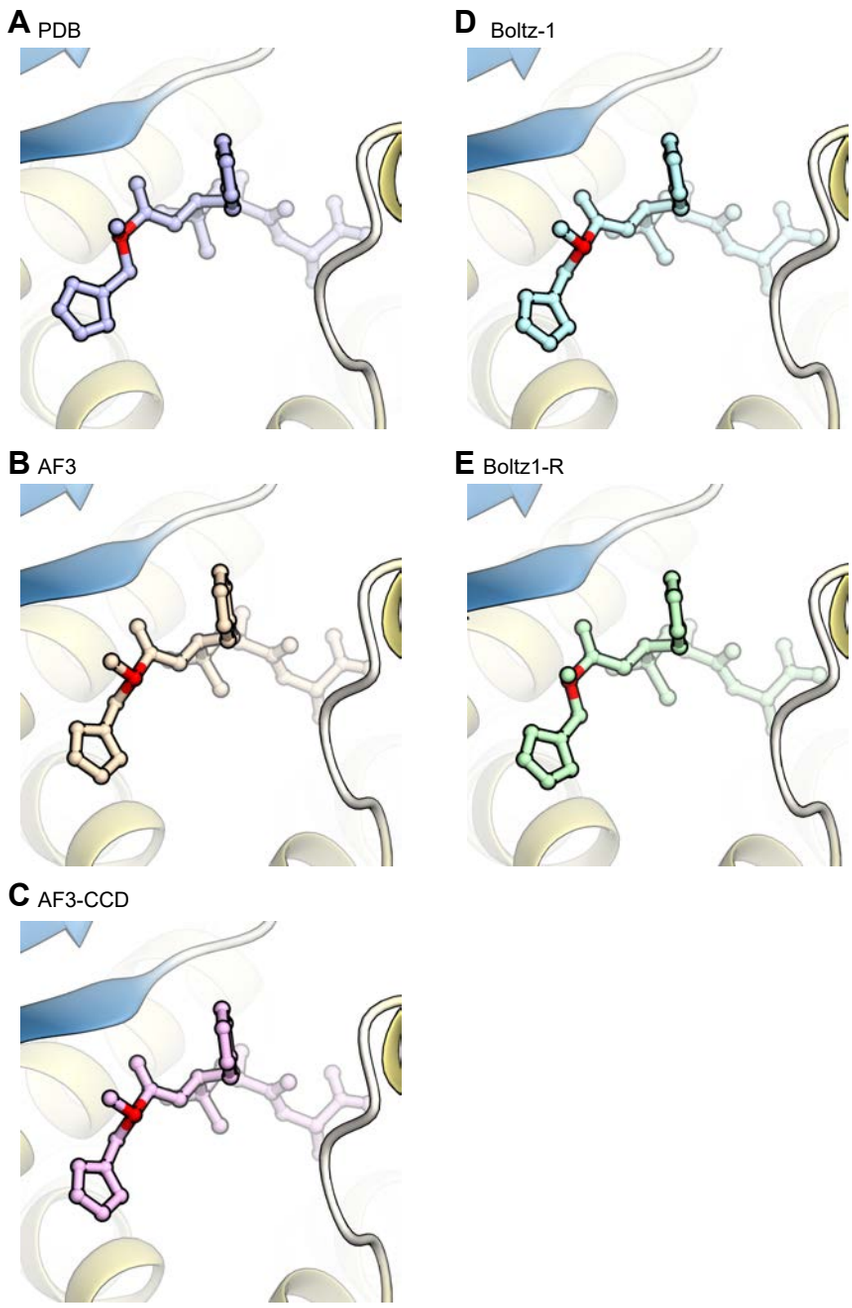

Fig 2 (4bxk)

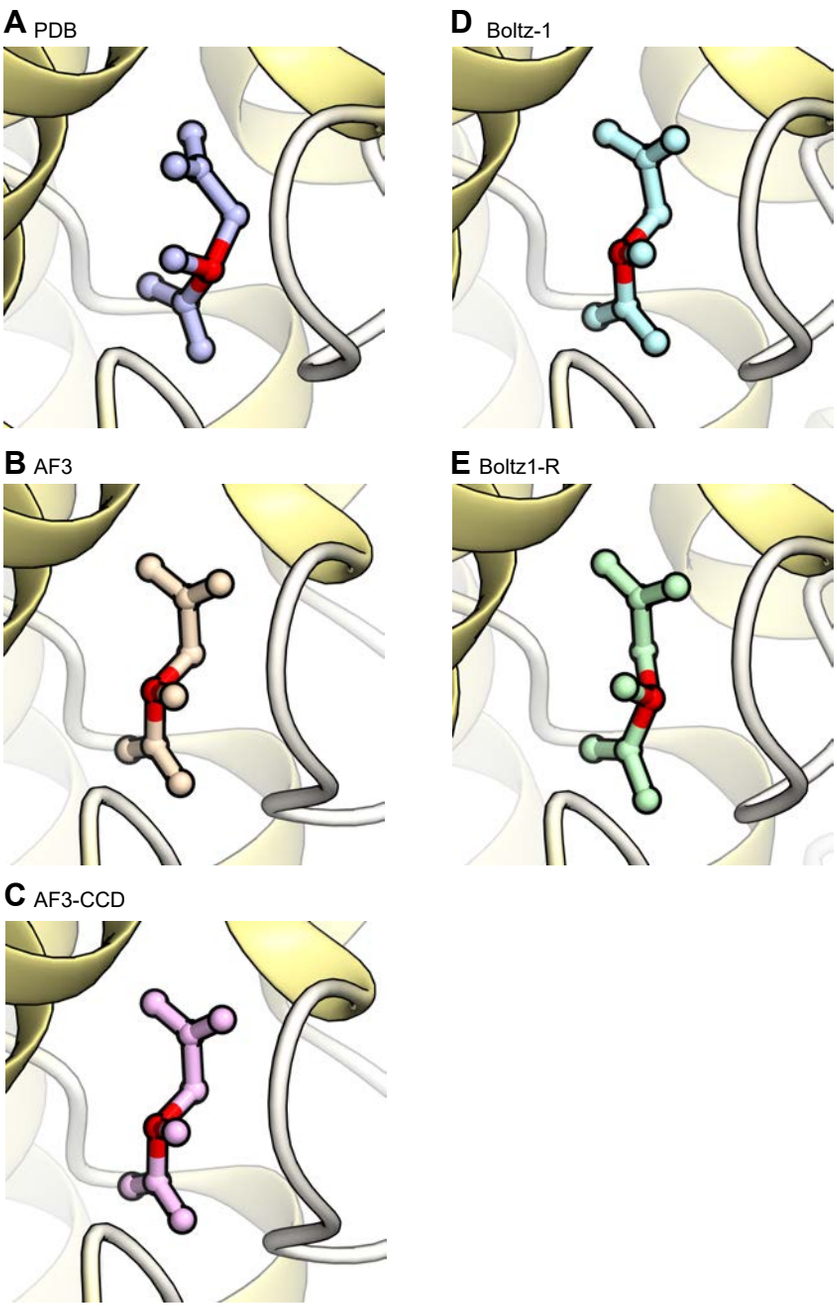

Fig 3 (6r7r)

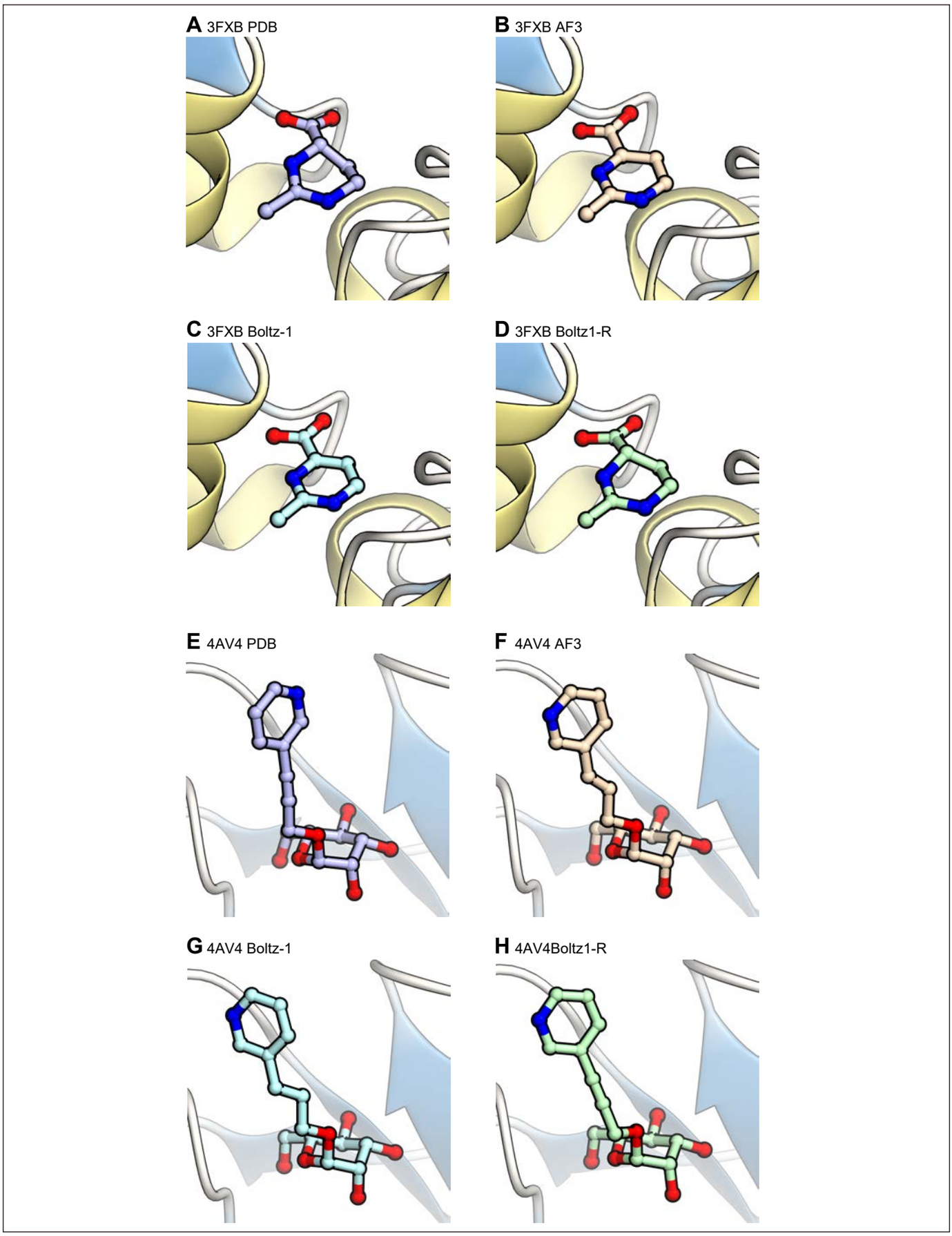

Fig 4 (3fxb,4av4)